



Synthesis of Z-scheme $\text{Ag}_2\text{CrO}_4/\text{Ag}/\text{g-C}_3\text{N}_4$ composite with enhanced visible-light photocatalytic activity for 2,4-dichlorophenol degradation



Yan Gong, Xie Quan*, Hongtao Yu, Shuo Chen

Key Laboratory of Industrial Ecology and Environmental Engineering (Ministry of Education), School of Environmental Science and Technology, Dalian University of Technology, Dalian, 116024, China

ARTICLE INFO

Article history:

Received 10 May 2017

Received in revised form 8 July 2017

Accepted 26 July 2017

Available online 27 July 2017

Keywords:

Visible light photocatalysis

$\text{g-C}_3\text{N}_4$

Z-scheme

2,4-dichlorophenol degradation

ABSTRACT

Designing and construction of highly efficient Z-scheme photocatalytic systems has received growing attention because of their unique advantages of excellent photogenerated carrier separation ability, complementary light absorption property and high redox capacities, which made them highly promising in refractory organic pollutants removing in the field of wastewater treatment. In this study, a narrow band gap Ag-based semiconductor Ag_2CrO_4 with broad visible light response range ($\lambda < 688 \text{ nm}$), sufficient oxidation capability of photogenerated hole and excellent photogenerated carrier separation ability was chosen to couple with $\text{g-C}_3\text{N}_4$ for enhancing the photocatalytic activity of $\text{g-C}_3\text{N}_4$. A series of Z-scheme $\text{Ag}_2\text{CrO}_4/\text{Ag}/\text{g-C}_3\text{N}_4$ composites were synthesized via facile in-situ growth strategy and photoreduction approach, and their photocatalytic performances for 2,4-dichlorophenol (2,4-DCP) degradation were evaluated under visible light irradiation ($\lambda > 420 \text{ nm}$). Benefiting from the broadband light utilization of the composite and efficient separation and transfer of photogenerated carriers, as well as the sufficient redox capacities of the photogenerated electrons and holes, the as-synthesized composites displayed remarkably enhanced photocatalytic activity for 2,4-DCP degradation, which was about 5.2 times as high as that over individual $\text{g-C}_3\text{N}_4$. Meanwhile, mechanism study through the active species trapping, electron spin resonance (ESR) experiments and band edge position estimation analysis provided evidences that the possible enhancing photocatalytic mechanism was ascribed to the Z-scheme. This work will shed light on design of other efficient $\text{g-C}_3\text{N}_4$ -based Z-scheme photocatalytic systems for application in environmental remediation.

© 2017 Elsevier B.V. All rights reserved.

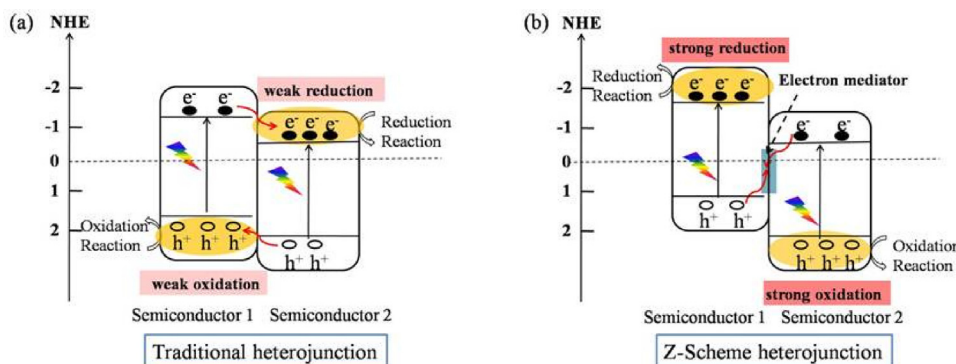
1. Introduction

Graphitic carbon nitride ($\text{g-C}_3\text{N}_4$), a metal-free polymeric semiconductor, has drawn extensively attention by virtue of its good thermal-chemical stability, electronic and optical characteristics [1–5]. Recently, it has been well known as a novel visible-light-driven photocatalyst in the field of solar hydrogen production and pollutant degradation [6–13]. However, the $\text{g-C}_3\text{N}_4$ obtained by the typically used thermal polymerization method usually suffers from moderate photocatalytic activities due to the rapid recombination of photogenerated electron-hole pairs and insufficient visible light absorption. The construction of $\text{g-C}_3\text{N}_4$ -based heterostructured photocatalysts has offered a reliable and facile strategy to overcome the above issue [14]. Incorporating appropriate photocatalyst

with $\text{g-C}_3\text{N}_4$ can promote the fast separation and transportation of photogenerated carriers and enlarge the spectral response range, which enhancing the photocatalytic activity of $\text{g-C}_3\text{N}_4$ [15]. To date, several $\text{g-C}_3\text{N}_4$ -based heterostructured photocatalysts (such as $\text{g-C}_3\text{N}_4/\text{TiO}_2$ [16], $\text{g-C}_3\text{N}_4/\text{ZnO}$ [17], $\text{g-C}_3\text{N}_4/\text{BiOBr}$ [18], and $\text{g-C}_3\text{N}_4/\text{BiPO}_4$ [19]; et al) have been reported. In the case of these hybrid composites, the photoinduced charge transfer is followed the traditional heterojunction-type way. As depicted in Scheme 1a, when both semiconductors are excited to generate electron–hole pairs, the photoexcited electrons (holes) can migrate from semiconductor 1 (semiconductor 2) with higher conduction band (CB) edge (lower valence band VB edge) to semiconductor 2 (semiconductor 1) with lower CB position (higher VB edge), resulting in accumulation of electrons on semiconductor 2 for a reduction reaction and holes on semiconductor 1 for an oxidation reaction, respectively. Thus the electrons and holes are spatially separated to effectively suppress charge recombination. Unfortunately, from the view of thermodynamics aspect, the redox ability of photoex-

* Corresponding author.

E-mail address: quanxie@dlut.edu.cn (X. Quan).



Scheme 1. Charge separation in various heterostructure-type photocatalytic systems.

cited electrons and holes on reaction sites are weakened, indicating the lower redox ability of this type heterostructure which is not enough to provide sufficient energy to trigger the surface redox reaction. Very recently, the construction of artificial Z-scheme photocatalytic system is deemed to be an ideal and effective means to solve the aforementioned problems [15,20]. The Z-scheme photocatalytic system is generally composed of two semiconductors with an electron mediator. As shown in Scheme 1b, the photogenerated electrons and holes in semiconductor 1 component possess strong reducing ability but weak oxidizing ability. On the contrary, the photogenerated carriers in semiconductor 2 component exhibit strong oxidizing ability but weak reducing ability. By quenching the photogenerated electrons and holes with weaker redox ability on the different moieties through the redox mediators, the resulting photogenerated carriers with strong redox ability can be used to participate in the surface reaction. It can not only inhibit the undesirable electron-hole recombination, but can also preserve excellent redox ability.

Up to now, several g-C₃N₄-based Z-scheme systems have been successfully prepared for enhancing photocatalytic activity of g-C₃N₄, including Ag@AgBr/g-C₃N₄ [21], g-C₃N₄/Au/CdS [22], g-C₃N₄/RGO/Bi₂WO₆ [23]; et al. Among these, Ag-containing photocatalysts have been shown to significantly promote the photocatalytic activity of g-C₃N₄ with Z-scheme by using noble metal Ag as the electron mediator [24,25]. It has been reported that the Ag₃PO₄/g-C₃N₄ exhibited enhanced photocatalytic CO₂ reduction performance by a Z-scheme mechanism [24]. However, Ag₃PO₄, with band gap \sim 2.4 eV, can only absorb part of visible light with the wavelength shorter than 460 nm which limits its utilization in solar-energy conversion. Therefore, it is necessary to construct a g-C₃N₄-based Z-scheme system with a narrow band gap Ag-based semiconductor photocatalyst for increasing utilization of solar energy.

Recently, Ag₂CrO₄, a narrow band gap semiconductor ($E_g \sim 1.8$ eV), has been explored as a novel Ag-based photocatalyst with superior photocatalytic activity for dyes and gaseous benzene degradation under visible light irradiation [2–30]. The large optical absorption coefficient of Ag₂CrO₄ implies its intensive visible-light absorption ability ($\lambda < 688$ nm). Theoretical calculation results reveal that Ag₂CrO₄ possesses excellent photogenerated carrier transfer and separation ability (small effective mass of charge carrier and striking difference in mobility of electrons and holes), which is advantageous for the carrier transfer to surface to participate in photocatalytic reactions [30]. What's more, the CB and VB edge potential of Ag₂CrO₄ are located at +0.47 V and +2.27 V respectively [31], indicating that the photogenerated holes have strong oxidation ability to decompose organic pollutants whereas the photogenerated electrons possess weak reduction capability. It has been reported that the photogenerated electron in the CB of Ag-containing photocatalysts can reduce the surface

Ag⁺ into metallic Ag [24,31]. The formed metallic Ag at the contact interface between Ag₂CrO₄ and g-C₃N₄ may serve as the electron mediator for charge carrier transfer when Ag₂CrO₄ and g-C₃N₄ combined together as a heterostructure composite. Enlightened by the above analysis, it is possible to construct a Z-scheme Ag₂CrO₄/g-C₃N₄ composite photocatalysts by using Ag as an electron-mediator.

In the present study, we have prepared the Z-scheme Ag₂CrO₄/g-C₃N₄ composite photocatalysts through facile precipitation method and photoreduction approach in a two-step procedure. The photocatalytic performance was evaluated by degradation of 2,4-DCP under visible light irradiation ($\lambda > 420$ nm). The separation mechanism of photogenerated electrons and holes in the hybrid photocatalyst was investigated through the active species trapping experiments and electron spin resonance (ESR) analysis as well as band edge position estimation.

2. Experimental section

2.1. Preparation of g-C₃N₄ and Ag₂CrO₄/Ag/g-C₃N₄

All chemicals used in this work were of analytical grade without further purification. The g-C₃N₄ was synthesized by typical thermal treatment of melamine according to the previous study [32]. Typically, 5 g melamine placed in a covered alumina crucible was heated in a muffle furnace at 550 °C for 4 h with a heating rate of 5 °C/min in air. After being cooled to room temperature, the obtained yellow block products were ground into powder for further use.

For preparation of the Ag₂CrO₄/Ag/g-C₃N₄ composite, 0.1 g of g-C₃N₄ powder was first dispersed in 100 mL of deionized water with ultrasonic treatment for 30 min, and then different amounts of AgNO₃ were added in the aqueous suspension and stirred for 12 h in the dark. Subsequently, a certain amount of K₂CrO₄ solution was added dropwise into the above solution under vigorous stirring. After stirring for 4 h, the precipitate was irradiated by a 500 W Xe lamp for 0.5 h. The obtained solid product was collected by centrifugation, washed with distilled water and ethanol for several times, and finally dried in an oven at 60 °C for 24 h. In this manner, the Ag₂CrO₄ to g-C₃N₄ with different weight ratios (i.e., 1%, 5%, 10%, 20%, and 30%) were obtained and denoted as 1ACN, 5ACN, 10ACN, 20ACN, and 30ACN, respectively. The counterpart g-C₃N₄ was also treated in the same manner without adding AgNO₃ and K₂CrO₄.

2.2. Characterization

The crystal structure of samples was investigated by using an X-ray diffractometer (XRD, Shimadzu LabX XRD-6000). The morphologies of samples were observed by field emission scanning electron microscope (SEM, Hitachi Co., Japan S-4800) and transmission electron microscopy (TEM FEI-Tecnai G² F30). And the optical

absorption properties was investigated by diffuse reflectance spectra (DRS) using a UV–Vis spectrophotometer (Shimadzu, UV-2450). X-ray photoelectron spectroscopy (XPS) measurements were performed on a Thermo Scientific ESCALAB 250 instrument with Al K α source. The total organic carbon (TOC) concentration was determined by a TOC auto analyzer (Analytik Jena, multi N/C 2100). Electron spin resonance (ESR) signals of spin-trapped paramagnetic species with 5,5-dimethyl-1-pyrroline-N-oxide (DMPO) were conducted with a Bruker A200 spectrometer. The photoelectrochemical performances were tested in 0.5 M Na₂SO₄ solution on a CHI 660D electrochemical system (Shanghai, China) using a standard three-electrode cell (working electrode, Pt counter electrode and standard calomel electrode (SCE)). The working electrode was prepared as follows: 5 mg of as-prepared photocatalyst was suspended in 1 mL dimethylformamide (DMF) with 10 μ L of Nafion solution to produce slurry, which was then dip-coated onto a 2 cm \times 2 cm indium-tin oxide (ITO) glass and annealed at 200 °C for 2 h under Ar.

2.3. Photocatalytic reactions

The photocatalytic activity of Ag₂CrO₄/Ag/g-C₃N₄ composites was evaluated by degradation of 2, 4-DCP aqueous solution under visible light irradiation. A 500W high pressure xenon lamp (CHF-XM35-500W, Beijing Changtu Co.) was used as the light source, and wavelengths below 420 nm were cut off by a visible light cut-off filter. A digital radiometer of model FZ-A (Photoelectric Instrument Factory Beijing Normal University) was used to ensure the incident visible-light intensity was about 100 mW/cm². Prior to irradiation, 50 mg photocatalyst was added into 50 ml 2, 4-DCP solution (10 mg/L) and stirred in dark for 1 h to achieve adsorptive equilibrium. After desired intervals, samples were collected and removed photocatalyst for subsequent analysis. The concentration of 2, 4-DCP was determined by a high performance liquid chromatography (Waters 2695). A Discovery C18 column was used, and the analysis was carried out with a 70/30 (v/v) methanol/water mobile phase at a flow rate of 1.0 mL/min. To investigate the active species generated in the photocatalytic degradation process, the experiments of active free radicals capture were studied by using t-butanol (TBA), ethylenediamine tetraacetic acid disodium salt (EDTA-2Na) and p-benzoquinone(BQ) as the scavengers for hydroxyl radical ($\cdot\text{OH}$), hole and $\cdot\text{O}_2^-$, respectively.

3. Results and discussion

3.1. Structure and Morphology of Ag₂CrO₄/Ag/g-C₃N₄ photocatalysts

Typical XRD patterns of g-C₃N₄, Ag₂CrO₄ and Ag₂CrO₄/Ag/g-C₃N₄ composites with different weight ratios of Ag₂CrO₄ are displayed in Fig. 1. Two characterization peaks of g-C₃N₄ appear at 27.5° and 13.1° are corresponded to (002) and (100) diffraction planes. The strong XRD peak at 27.5° is indicative of the interplanar stacking of aromatic systems, while the peak at 13.1° is assigned to the interplanar structural packing motif (100) of tri-s-triazine units [3–35]. All diffraction peaks of the as-prepared Ag₂CrO₄ coincide well with the orthorhombic phase of Ag₂CrO₄ (JCPDS No. 26-0952) [29,31]. From the XRD patterns of Ag₂CrO₄/Ag/g-C₃N₄ composite samples, both of diffraction peaks corresponding to g-C₃N₄ and Ag₂CrO₄ can be observed without other impurity phases, indicating that the Ag₂CrO₄ has been successfully introduced on the g-C₃N₄ to form hybrid composite. In addition, the intensities of diffraction peaks of g-C₃N₄ become weaker with increasing the contents of Ag₂CrO₄ in the Ag₂CrO₄/Ag/g-C₃N₄ composite, reflecting their contents in the hybrids. It should be noted that, although all the

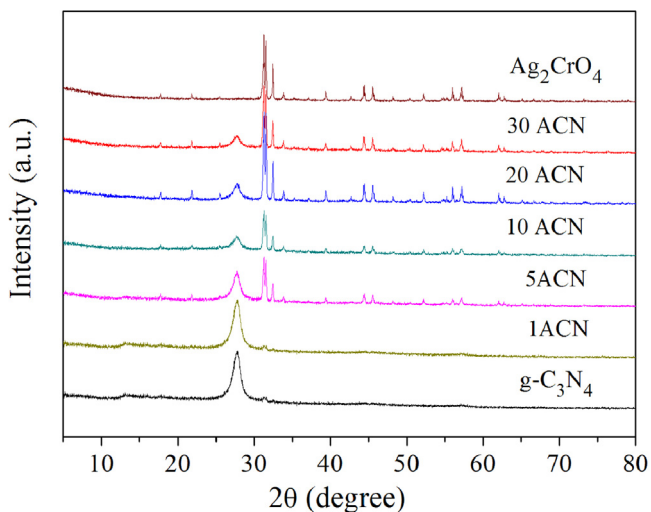


Fig. 1. XRD patterns of Ag₂CrO₄, g-C₃N₄, and Ag₂CrO₄/g-C₃N₄.

samples were irradiated by Xe lamp for 0.5 h, no diffraction peaks of metallic Ag specie can be observed, indicating that the photo-induced formed Ag nanoparticles may have a small particle size and low amount, which could not be detected by the XRD method. The similar results have been reported in the previous studies [24,36].

The morphologies of as-synthesized samples were characterized by SEM and TEM. From Fig. 2a and 3a, it can be observed that the g-C₃N₄ is composed of crumpled stacking layered structure with smooth surface. Fig. 2b and 3b demonstrates that the as-synthesized Ag₂CrO₄ mainly present as nanoparticles with average size of 400 nm–1 μ m and the corresponding high-resolution transmission electron microscopy (HRTEM) images display that the lattice spacing value of the formed nanoparticles is determined to 0.288 nm, corresponding to the (220) crystal plane of Ag₂CrO₄ (Fig. 3d). After introducing Ag₂CrO₄ into the g-C₃N₄, as shown in Fig. 2c and d, Ag₂CrO₄/Ag/g-C₃N₄ composites appears some nanoparticles uniformly anchored on the surface of g-C₃N₄, leading to the formation of a heterostructure. The TEM image of Ag₂CrO₄/Ag/g-C₃N₄ sample, as displayed in Fig. 3c, illustrates that the Ag₂CrO₄ nanoparticles were well interwoven among g-C₃N₄ and the formed heterostructure was further verified by the corresponding HRTEM images of the Ag₂CrO₄/Ag/g-C₃N₄ composite as shown in Fig. 3e and f. The Ag₂CrO₄ particles with high crystallinity can be notarized by the lattice spacing values of 0.288 nm which is matched with the (220) crystal plane of Ag₂CrO₄, and the g-C₃N₄ presented low crystallinity feature due to its polymer nature. The HRTEM image of Fig. 3f shows a distinguished interface with well-defined boundary between the phase of Ag₂CrO₄ and g-C₃N₄, manifesting that a heterojunction might be formed. Moreover, several distinct nanoparticles (marked by the red arrow) with average size of 2–5 nm formed between the Ag₂CrO₄ nanoparticles and g-C₃N₄ can be observed in Fig. 3e and the HRTEM image of Fig. 3f further revealed that the lattice fringes of the formed particles between Ag₂CrO₄ and g-C₃N₄ can be assigned to Ag (111) plane [37,38], which gives a direct evidence for the existing of metallic Ag formed in the hybridized structure. The formed heterostructure would facilitate the transfer of photogenerated carriers.

The elements composition and chemical states of Ag₂CrO₄, g-C₃N₄ and Ag₂CrO₄/Ag/g-C₃N₄ composite were investigated by X-ray photoelectron spectroscopy (XPS) measurements. As shown in Fig. 4a, the C 1 s spectrum of g-C₃N₄ exhibits two distinct peaks at 284.6 and 287.7 eV, corresponding to the graphitic carbon (sp² C–C bonds) and the sp² hybridized carbon in N-containing aromatic ring (N=C=N) in graphitic carbon nitride[24,34]. And these

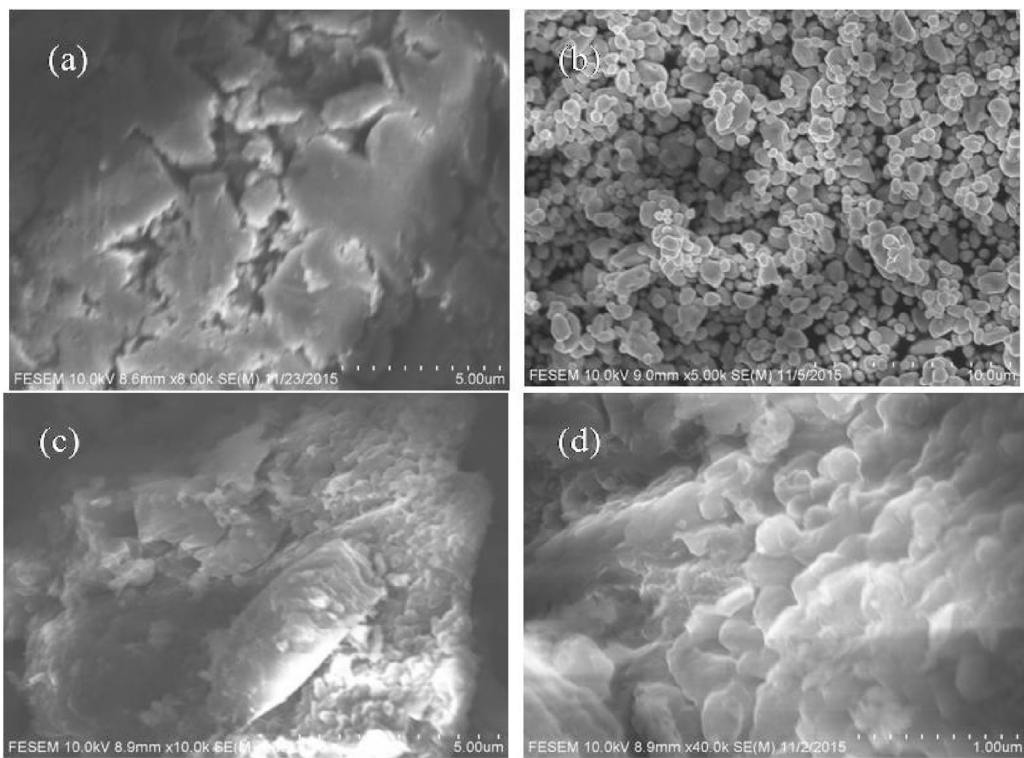


Fig. 2. SEM images of (a) $\text{g-C}_3\text{N}_4$, (b) Ag_2CrO_4 and (c,d) $\text{Ag}_2\text{CrO}_4/\text{Ag}/\text{g-C}_3\text{N}_4$.

two peaks are also observed in the C 1 s spectrum of $\text{Ag}_2\text{CrO}_4/\text{Ag}/\text{g-C}_3\text{N}_4$, confirming the existence of a $\text{g-C}_3\text{N}_4$ phase in the composite. Fig. 4b displays the Cr 2p spectrum of Ag_2CrO_4 and $\text{Ag}_2\text{CrO}_4/\text{Ag}/\text{g-C}_3\text{N}_4$, the peaks at 579.7 eV and 588.8 eV are ascribed to Cr^{6+} [39]. It should note that the binding energy (BE) of C 1 s and Cr 2p are not changed. On contrast, For N 1 s spectra (Fig. 4c), the BE of N 1 s shifts about 0.4 eV to higher binding energies, suggesting that the chemical microenvironment of N atoms in C-N-C and N-(C)₃ groups has changed after $\text{g-C}_3\text{N}_4$ hybridizes with Ag_2CrO_4 [24]. As reported in previous work [33,34], the change of binding energy in XPS spectra can be ascribed to the intense interaction between Ag_2CrO_4 and $\text{g-C}_3\text{N}_4$, implying the existence of heterostructure interaction in the as-synthesized composite. Fig. 4d and e display the Ag 3d spectra of Ag_2CrO_4 and $\text{Ag}_2\text{CrO}_4/\text{Ag}/\text{g-C}_3\text{N}_4$. To gain more insight into the chemical states of Ag species, the Ag 3d spectra were deconvoluted by Gaussian-Lorenzian analysis method. The Ag 3d_{5/2} and 3d_{3/2} BE of Ag_2CrO_4 are located at 367.7 eV and 373.6 eV, respectively, corresponding to Ag^+ in Ag_2CrO_4 [31]. For the $\text{Ag}_2\text{CrO}_4/\text{Ag}/\text{g-C}_3\text{N}_4$ composite, two new peaks at 368.6 eV and 374.5 eV assigned to metallic Ag can be observed, further confirming the existence of metallic Ag in the $\text{Ag}_2\text{CrO}_4/\text{Ag}/\text{g-C}_3\text{N}_4$ composite [21,24,31,35]. The formed Ag nanoparticles may origin from the photoreduction procedure in the synthetic process.

3.2. Optical properties of $\text{Ag}_2\text{CrO}_4/\text{Ag}/\text{g-C}_3\text{N}_4$ photocatalysts

The optical properties of as-synthesized samples were studied by UV–Vis diffuse reflection spectroscopy. As shown in Fig. 5a. Obviously, the $\text{g-C}_3\text{N}_4$, Ag_2CrO_4 and all $\text{Ag}_2\text{CrO}_4/\text{Ag}/\text{g-C}_3\text{N}_4$ samples display visible-light-response ability. The absorption edge of the $\text{g-C}_3\text{N}_4$ is located at around 460 nm. And the Ag_2CrO_4 shows strong adsorption over a wide spectra region from UV to visible light with wavelength range up to 680 nm, indicating its broad visible-light absorption range. Considering that both of $\text{g-C}_3\text{N}_4$ [23,34] and Ag_2CrO_4 [29,30] are indirect band gap semiconductors, the band gaps of as-synthesized $\text{g-C}_3\text{N}_4$ and Ag_2CrO_4 can be deter-

mined from the intercept of the tangents to the plots of $(\alpha h\nu)^{1/2}$ vs. photon energy. As displayed in Fig. 5b, the calculated band gaps of $\text{g-C}_3\text{N}_4$ and Ag_2CrO_4 are 2.8 eV and 1.78 eV, respectively, which agrees well with previous researches [30,34,39,40]. In the absorption spectra of $\text{Ag}_2\text{CrO}_4/\text{Ag}/\text{g-C}_3\text{N}_4$ composites, it can be clearly found that the absorption edge of the composites shifts regularly to long wavelength, and the absorption intensity of the composites is also gradually strengthened with increased Ag_2CrO_4 content, suggesting the enhanced light harvesting in visible light region after Ag_2CrO_4 loading on the $\text{g-C}_3\text{N}_4$.

Photoelectrochemical performance is considered to be efficient evidence for evaluating the photogenerated charge separation in the composite. The transient photocurrent responses of $\text{g-C}_3\text{N}_4$ and $\text{Ag}_2\text{CrO}_4/\text{Ag}/\text{g-C}_3\text{N}_4$ were recorded over several on-off cycles under visible-light irradiation and shown in Fig. 6a. The photocurrent responses of all samples are reproducible during three on-off intermittent irradiation cycles. The pristine Ag_2CrO_4 possessed higher photocurrent intensity than that of $\text{g-C}_3\text{N}_4$, which indicates that the Ag_2CrO_4 present superior separation ability of photogenerated carriers in compared with $\text{g-C}_3\text{N}_4$. This was attributed to the intensive visible-light absorption ability and excellent charge separation and transfer ability of Ag_2CrO_4 . Apparently, the photocurrent intensity of $\text{Ag}_2\text{CrO}_4/\text{Ag}/\text{g-C}_3\text{N}_4$ composite ($0.8 \mu\text{A}/\text{cm}^{-2}$) is about 4.4 times as high as that of the $\text{g-C}_3\text{N}_4$ electrode, indicating higher separation efficiency of photogenerated carriers under visible-light irradiation. Moreover, electrochemical impedance spectroscopy were conducted to investigate the charge transfer properties of $\text{g-C}_3\text{N}_4$ and $\text{Ag}_2\text{CrO}_4/\text{Ag}/\text{g-C}_3\text{N}_4$. As shown in Fig. 6b, the EIS Nyquist plot of $\text{Ag}_2\text{CrO}_4/\text{Ag}/\text{g-C}_3\text{N}_4$ composite exhibits a much smaller arc radius than that of $\text{g-C}_3\text{N}_4$ alone, implying the lower charge transfer resistance of $\text{Ag}_2\text{CrO}_4/\text{Ag}/\text{g-C}_3\text{N}_4$ composite. Meanwhile, it is noteworthy that the charge transfer resistance of Ag_2CrO_4 is lower than that of the $\text{g-C}_3\text{N}_4$, which indicates that the Ag_2CrO_4 presents lower photogenerated carrier recombination rate in compared with $\text{g-C}_3\text{N}_4$. Apparently, the introduction of Ag_2CrO_4 can enhance sep-

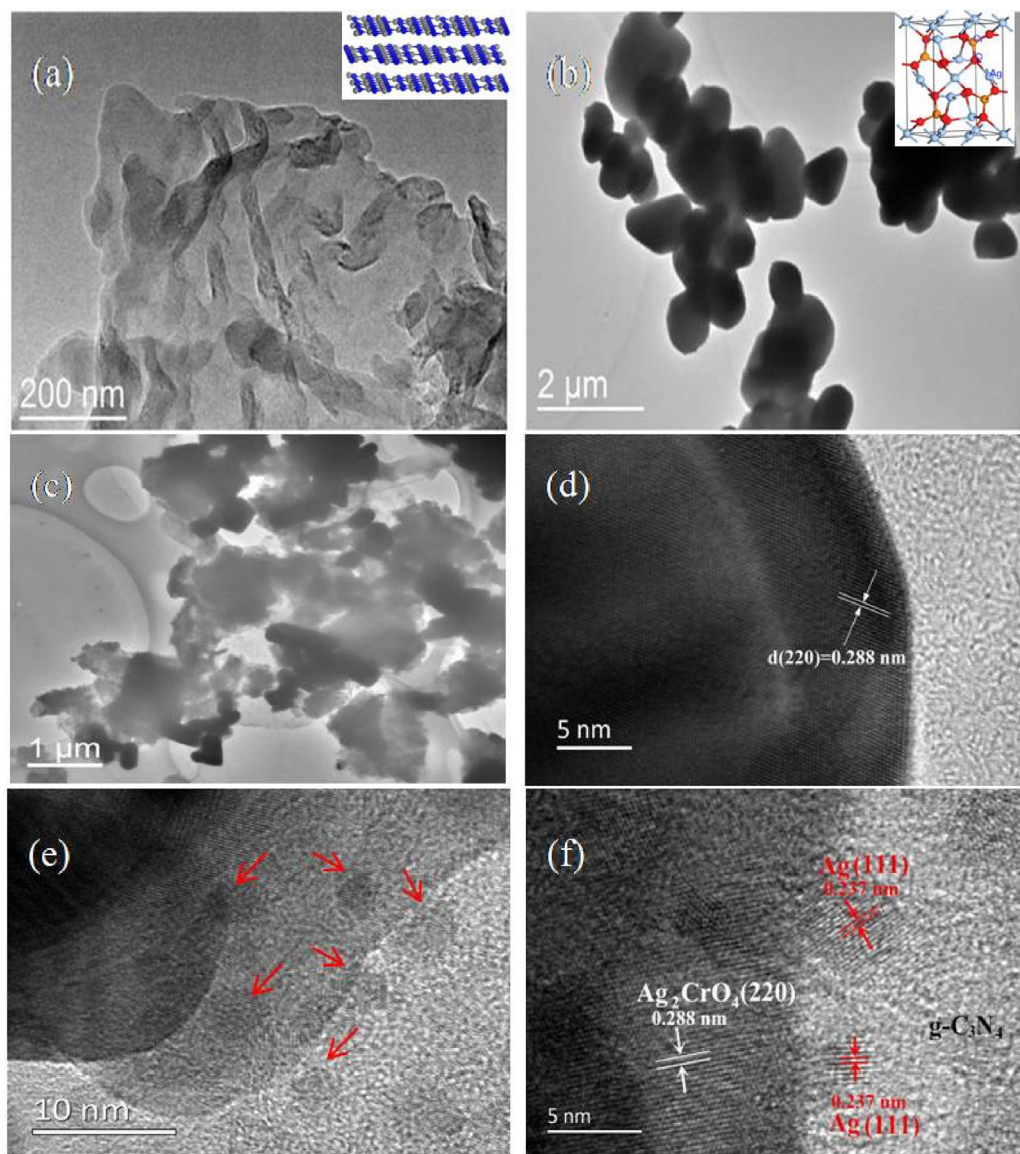


Fig. 3. TEM images of (a) g-C₃N₄; (b) Ag₂CrO₄; (c) Ag₂CrO₄/Ag/g-C₃N₄ and HRTEM images of (d) Ag₂CrO₄ and (e, f) Ag₂CrO₄/Ag/g-C₃N₄.

aration efficiency of photoinduced charge carriers in g-C₃N₄, which may force more photoinduced electrons and holes to participate in the surface reaction. And it is highly anticipated that the composite may possess a better photocatalytic activity.

3.3. Photocatalytic activity

The photocatalytic activities of g-C₃N₄ and as-prepared Ag₂CrO₄/Ag/g-C₃N₄ composites samples were evaluated by the degradation of 2,4-DCP as a model pollutant under visible light irradiation ($\lambda > 420$ nm). As shown in Fig. 7a, Prior to irradiation, the adsorption-desorption equilibriums of all samples are analyzed in dark for 1 h. The blank test without the catalyst reveals that the photolysis of 2,4-DCP can be negligible. The individual g-C₃N₄ shows relatively low photocatalytic activity for 2,4-DCP degradation and only 31% of 2,4-DCP can be removed after 2 h under visible light irradiation. Significantly, the Ag₂CrO₄/Ag/g-C₃N₄ composites possess higher photocatalytic activity than that of g-C₃N₄ alone and the content of Ag₂CrO₄ in the composites exhibits a significant effect on the 2,4-DCP removal efficiency. The degradation efficiency increased gradually from 52% to 94% as Ag₂CrO₄

content increased from 1% to 10% in the composite and then decreased to 63% as Ag₂CrO₄ content further increased to 30%. The 10% Ag₂CrO₄/Ag/g-C₃N₄ (10ACN) composite exhibited the highest photocatalytic activity and a higher Ag₂CrO₄ content lead to a decreased activity. This may be ascribed to the reduced light absorption by g-C₃N₄. In order to confirm the role of the formed heterostructure in composite, the photocatalytic activity of the mechanical mixtures (Ag₂CrO₄ and g-C₃N₄ with a weight ratio of 1:10) as counterpart was measured and the mixed powders also shows limited photocatalytic activity, indicating that the loosely contacted between Ag₂CrO₄ and g-C₃N₄ is insufficient for improving the photocatalytic performance of the composite. Thus it can be deduced that the improved photocatalytic activity of composites is ascribe to the strong interaction between the interfacial phases in formed hetersturcture composite. To further study the mineralization of 2,4-DCP in the photocatalytic reaction, the change of total organic carbon concentration was monitored and shown in Fig. 7b. Obviously, the TOC removal with Ag₂CrO₄/Ag/g-C₃N₄ (10ACN) composite reached 62% after 2 h reaction, which is higher than that of the g-C₃N₄ alone (19%). This result is matched with the

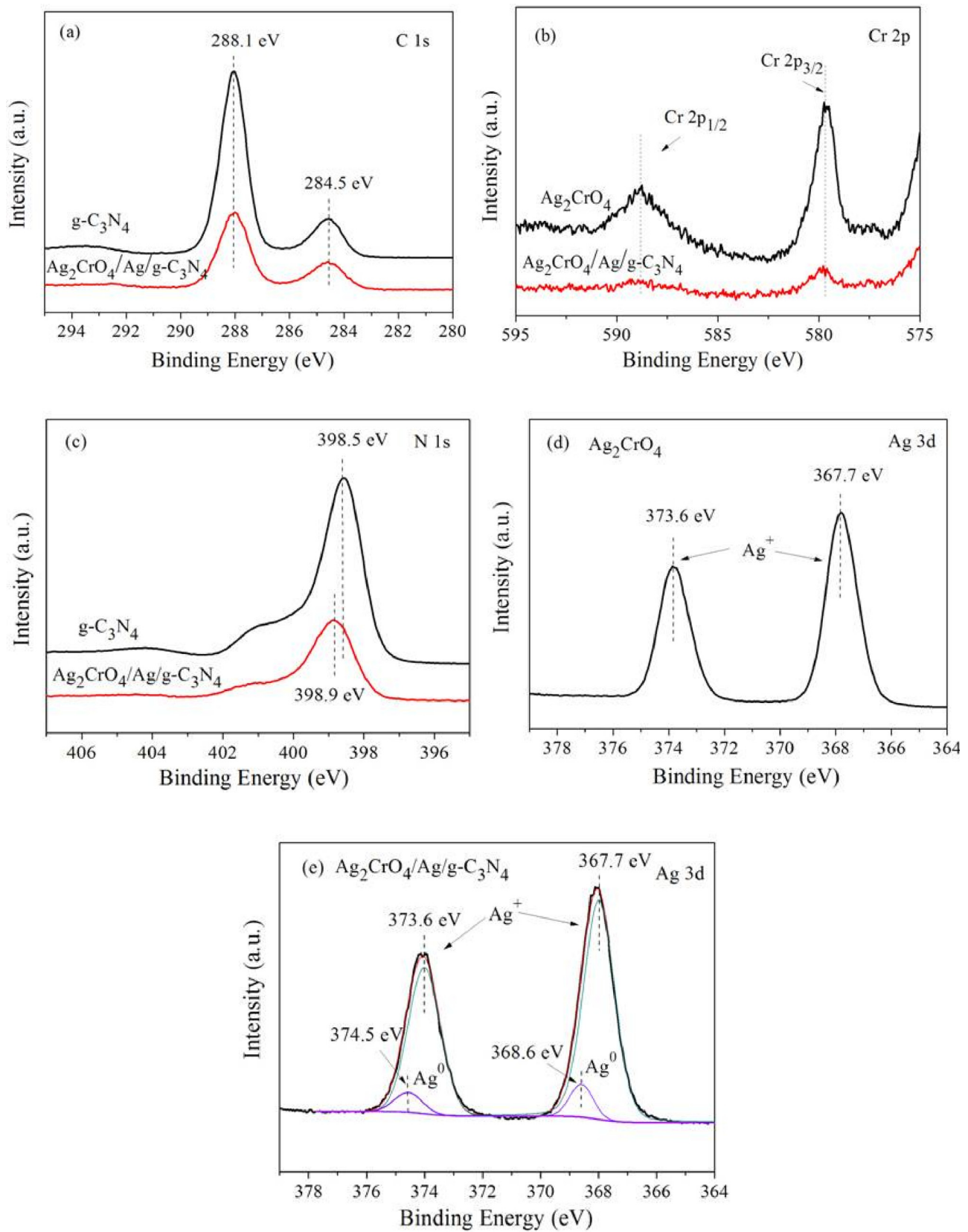


Fig. 4. XPS spectra of the $\text{Ag}_2\text{CrO}_4/\text{g-C}_3\text{N}_4$ composite: (a) the Ag 3d of Ag_2CrO_4 ; (b) the Ag 3d of $\text{Ag}_2\text{CrO}_4/\text{Ag}/\text{g-C}_3\text{N}_4$; (c) the Cr 2p of Ag_2CrO_4 and $\text{Ag}_2\text{CrO}_4/\text{Ag}/\text{g-C}_3\text{N}_4$; (d, e) the C 1s and N 1s of $\text{g-C}_3\text{N}_4$ and $\text{Ag}_2\text{CrO}_4/\text{Ag}/\text{g-C}_3\text{N}_4$.

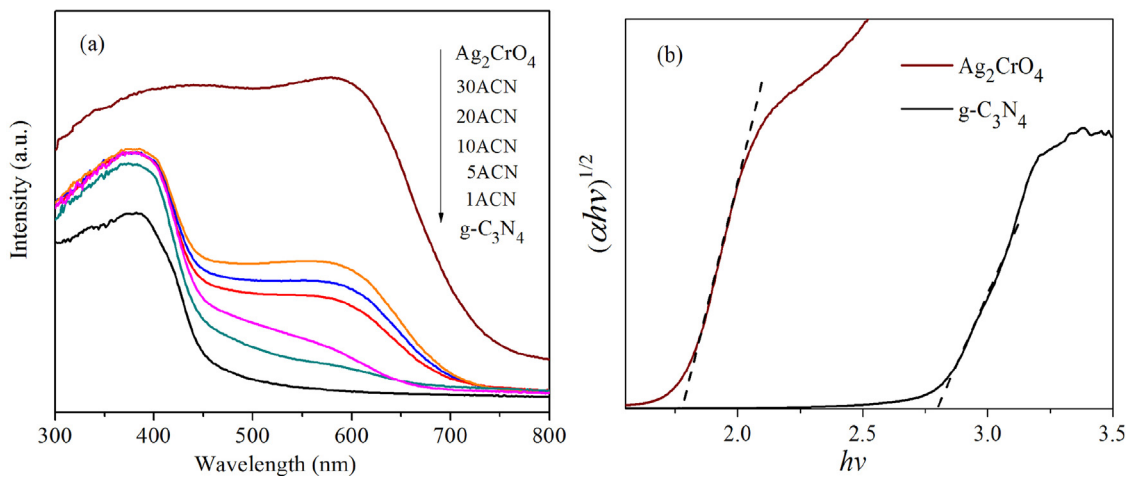


Fig. 5. (a) UV–Vis diffuse reflectance spectra of $\text{g-C}_3\text{N}_4$, Ag_2CrO_4 and $\text{Ag}_2\text{CrO}_4/\text{g-C}_3\text{N}_4$ photocatalysts and (b) the corresponding Tauc plot.

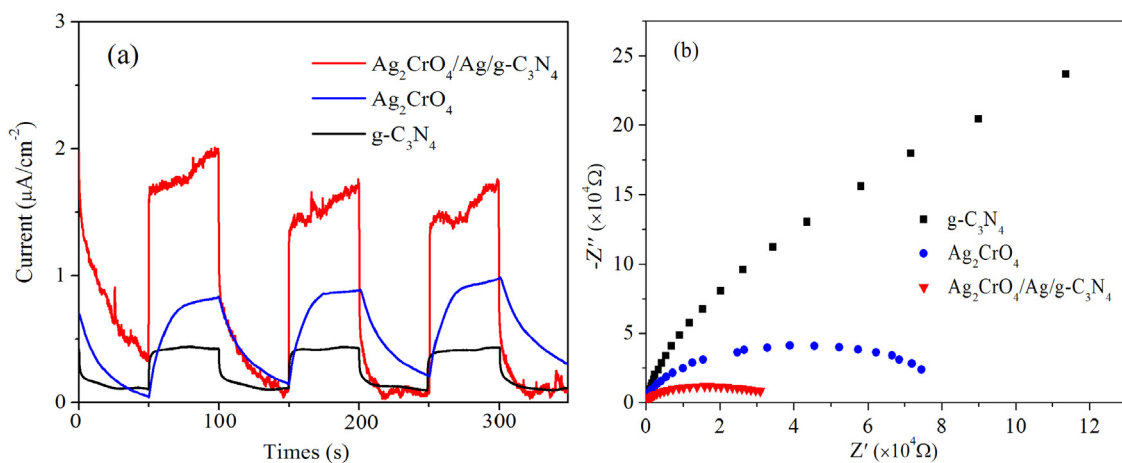


Fig. 6. (a) Transient photocurrent density and (b) electrochemical impedance spectroscopy of different sample electrodes.

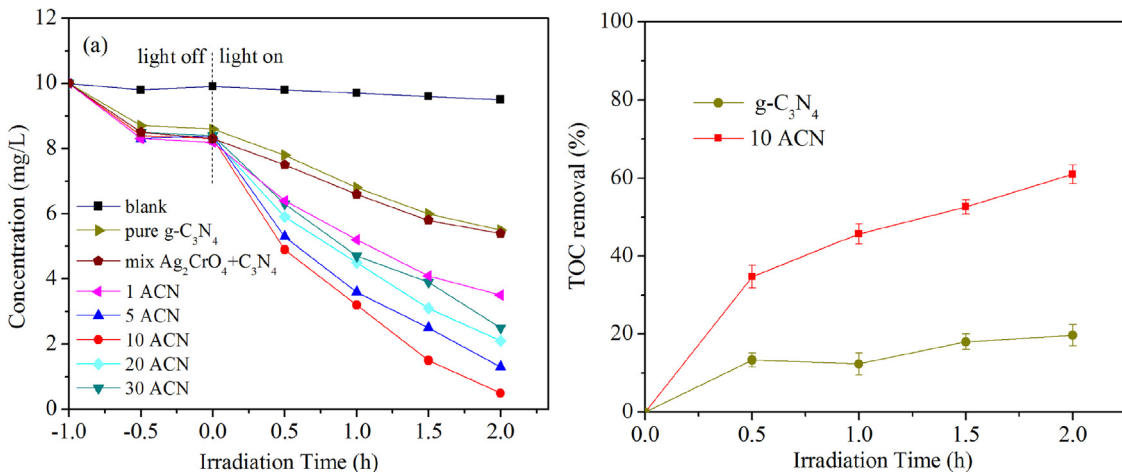


Fig. 7. (a) Photocatalytic activities of the 2,4-DCP degradation on $\text{g-C}_3\text{N}_4$ and $\text{Ag}_2\text{CrO}_4/\text{g-C}_3\text{N}_4$ with different Ag_2CrO_4 content under visible light irradiation and (b) TOC removal during the mineralization of 2,4-DCP.

degradation result, indicating that the $\text{Ag}_2\text{CrO}_4/\text{Ag}/\text{g-C}_3\text{N}_4$ composite possesses improved photocatalytic activity.

As shown in Fig. 8a and b, the photocatalytic reaction process of 2,4-DCP degradation over $\text{g-C}_3\text{N}_4$ and $\text{Ag}_2\text{CrO}_4/\text{Ag}/\text{g-C}_3\text{N}_4$ samples followed pseudo-first-order kinetics, and the slope of the fitting line is corresponding to the value of rate constant k . It clearly illustrated

that All $\text{Ag}_2\text{CrO}_4/\text{Ag}/\text{g-C}_3\text{N}_4$ samples displayed higher photocatalytic performance than that of $\text{g-C}_3\text{N}_4$ alone. The 10ACN composite showed the highest activity toward 2,4-DCP degradation with an apparent rate constant (k) of 0.91 h^{-1} , which was 5.2 times than that of $\text{g-C}_3\text{N}_4$. Meanwhile, as shown in Fig. 9a, the photocatalytic activity of 10ACN decreased slightly after five times of cycling test

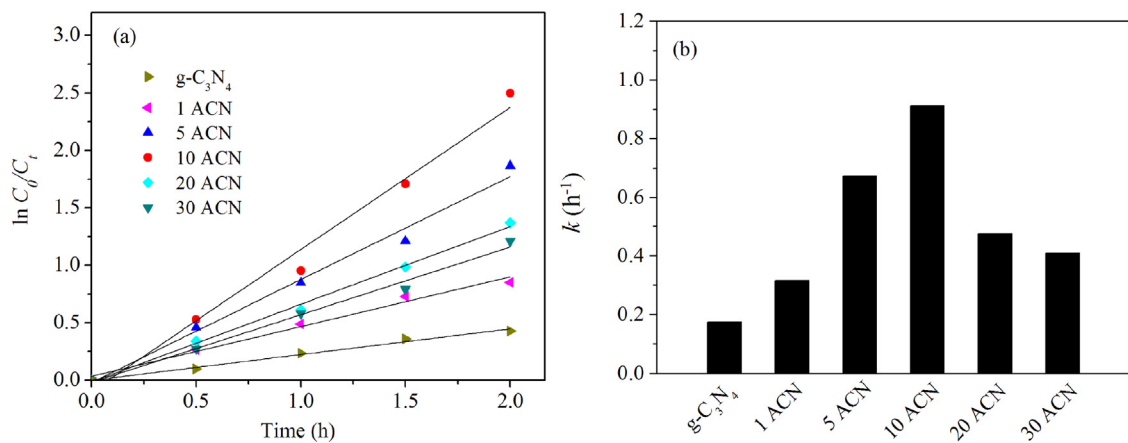


Fig. 8. (a) Variation curve of $\ln(C_0/C_t)$ with reaction time for the 2,4-DCP degradation; (b) Comparison of the kinetic constants of 2,4-DCP degradation with different samples under visible light irradiation.

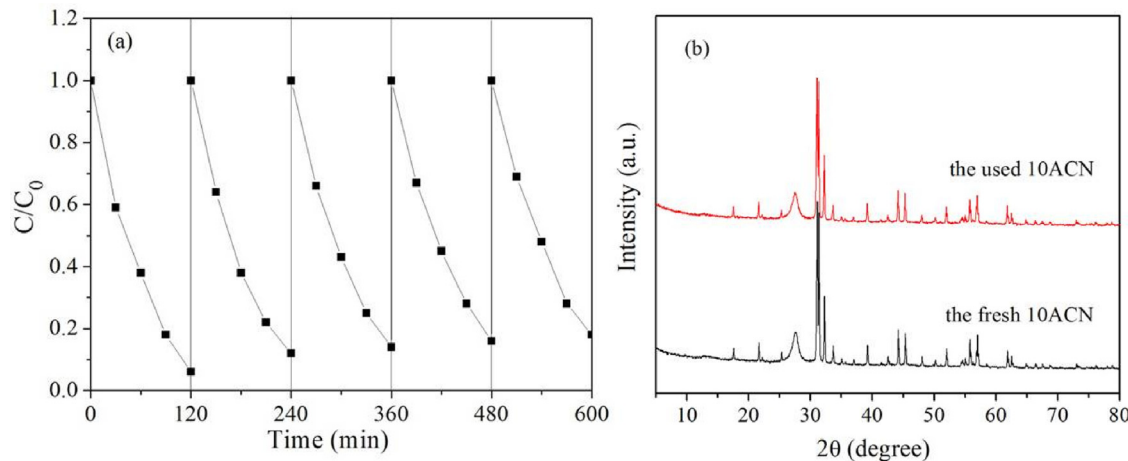


Fig. 9. (a) Cycling test of $\text{Ag}_2\text{CrO}_4/\text{Ag}/g\text{-C}_3\text{N}_4$ under visible light irradiation and (b) XRD patterns of the fresh and used 10ACN.

(~9%), indicating the robust photostability of composite. In addition, the XRD pattern of the used 10ACN sample was measured and compared with the fresh 10ACN to investigate the structures changes of the samples before and after photocatalytic reaction. There is no obvious discrepancy can be observed in Fig. 9b, suggesting that the crystal structure of the composite did not changed and the composite exhibited high stability.

3.4. Photocatalytic Mechanism

The active species trapping experiments for the 2,4-DCP degradation over $g\text{-C}_3\text{N}_4$ and $\text{Ag}_2\text{CrO}_4/\text{Ag}/g\text{-C}_3\text{N}_4$ samples were carried out to explore the enhancing photocatalytic mechanism. Fig. 10 shows the photocatalytic process of 10% $\text{Ag}_2\text{CrO}_4/\text{Ag}/g\text{-C}_3\text{N}_4$ with different quenchers. The t-butanol (TBA), p-benzoquinone (BQ) and EDTA-2Na were used as the quenchers for $\cdot\text{OH}$, $\cdot\text{O}_2^-$ and h^+ , respectively. After adding TBA, it shows negligible effect on the degradation rate of 2,4-DCP. On the other hand, the degradation rate of 2,4-DCP decreased rapidly after adding BQ and EDTA-2Na, respectively, indicating that $\cdot\text{O}_2^-$ and h^+ are the main active species in the photocatalytic processes.

It is well known that the band alignment plays an important role in a heterostructure photocatalyst with high photocatalytic ability. To exploits the band position of the $g\text{-C}_3\text{N}_4$ and Ag_2CrO_4 , Mott-Schottky test were used to estimate the positions of conduction band (CB). As shown in Fig. 11, both $g\text{-C}_3\text{N}_4$ and Ag_2CrO_4 are n-type

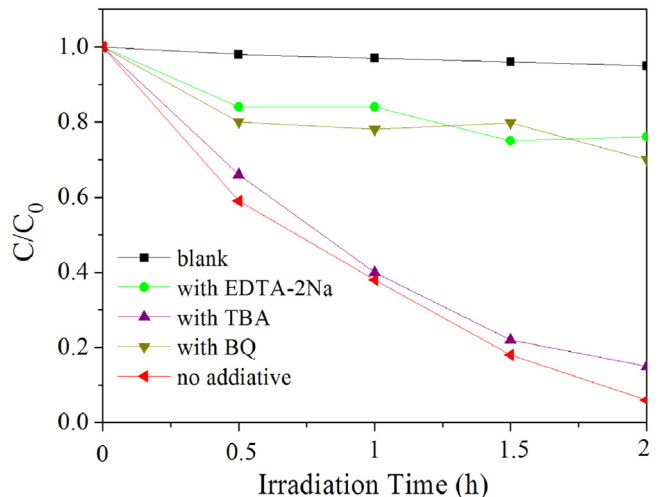
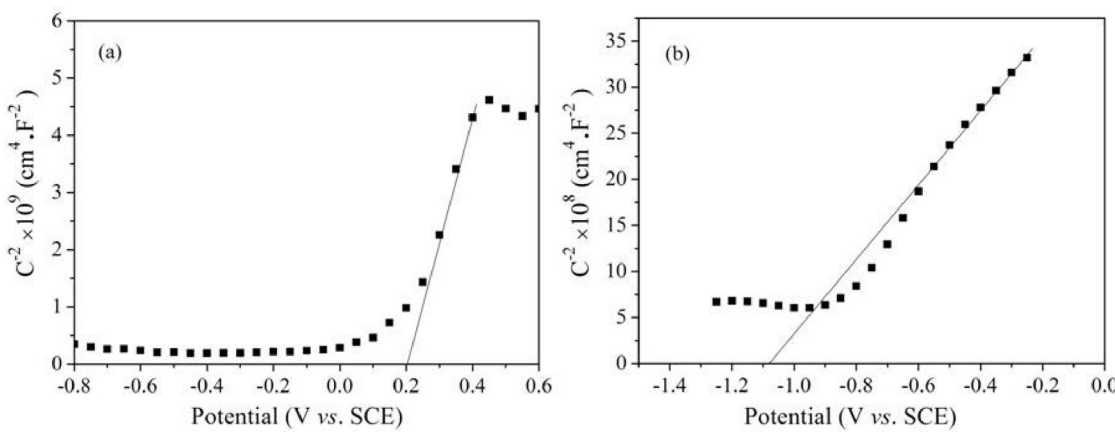
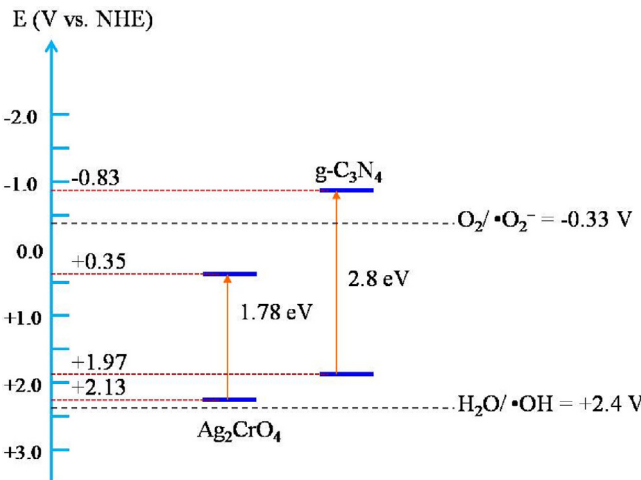


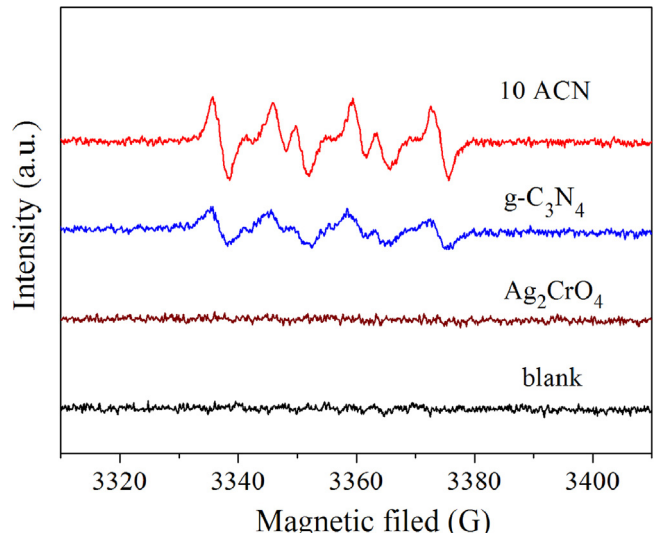
Fig. 10. Reactive species trapping experiments of $\text{Ag}_2\text{CrO}_4/\text{Ag}/g\text{-C}_3\text{N}_4$ under visible light irradiation.

semiconductors and the flat potentials of $g\text{-C}_3\text{N}_4$ and Ag_2CrO_4 are located at -1.07 and 0.21 V (vs SCE), which corresponds to -0.83 and 0.45 V (vs NHE) respectively. It has been accepted that the flat potential of n-type semiconductor is lower 0.1 eV than that of the conduction band [31,41,42], thus the conduction band potentials of

Fig. 11. Mott-Schottky plots of (a) Ag₂CrO₄ and (b) g-C₃N₄.Fig. 12. Schematic diagram of band structure and redox potential of Ag₂CrO₄ and g-C₃N₄.

g-C₃N₄ and Ag₂CrO₄ are estimated to be −0.83 and 0.35 V, respectively. The Ag₂CrO₄ possesses a more positive conduction band edge than that of the g-C₃N₄. Combing the result of CB potential and the band-gap values extrapolated by UV/Vis spectra (Fig. 5b), the band alignments of Ag₂CrO₄ and g-C₃N₄ can be drawn as illustrated in Fig. 12.

If the photogenerated carrier separation at the interfacial phases of the Ag₂CrO₄/Ag/g-C₃N₄ hybrids follows the traditional heterojunction-type mechanism [14,15,20], the photogenerated electrons in the CB of g-C₃N₄ would transfer to the CB of Ag₂CrO₄ to participate in the reduction reaction and the photogenerated hole would migrate from the VB of Ag₂CrO₄ to that of g-C₃N₄ for the oxidation reaction. Because the CB level of Ag₂CrO₄ is less negative than the •O₂⁻/O₂ potential (−0.33 V) [31], it is difficult for the photogenerated electron in the CB of Ag₂CrO₄ to reduce the adsorbed O₂ to produce •O₂⁻. Thus the introduction of Ag₂CrO₄ to g-C₃N₄ cannot significantly promote •O₂⁻ production. However, the reactive species trapping experiments have demonstrated that •O₂⁻ radicals play an important role in the photocatalytic process. Hence, if the photogenerated charge transfer is in accordance with the traditional heterojunction-type, it is unfavorable for the Ag₂CrO₄/Ag/g-C₃N₄ composite to form the active species. Therefore, from the above discussion, it could be proposed that the photogenerated charge transfer way may follow Z-scheme mechanism. In order to understand the presented reaction mechanism of the photogenerated electron-hole separation process more better,

Fig. 13. ESR signals of the DMPO-•O₂⁻ adducts in methanol system of various photocatalysts after 1 h visible-light irradiation.

the production of •O₂⁻ radicals in g-C₃N₄ and Ag₂CrO₄/Ag/g-C₃N₄ composite reaction system were detected by ESR under visible light irradiation [34,43,44]. Fig. 13 shows that the distinct characteristic peaks of DMPO-•O₂⁻ adducts for g-C₃N₄ and Ag₂CrO₄/Ag/g-C₃N₄ sample can be observed, indicating that •O₂⁻ radicals were generated on the surface of two samples after visible light irradiation. Furthermore, the •O₂⁻ signal intensity of the Ag₂CrO₄/g-C₃N₄ composite is obviously stronger than that of g-C₃N₄ alone, implying that the amount of •O₂⁻ radical generated on the surface of Ag₂CrO₄/Ag/g-C₃N₄ composite is higher than that of g-C₃N₄ under visible light irradiation. This result suggests that plenty of electrons in the CB of g-C₃N₄ participated in the reduction reaction for •O₂⁻ radical production.

Furthermore, to elucidate the mechanism of the charge transfer way in the composite, the photocatalytic activities and photoelectrochemical properties of the composite under irradiation with different wavelength light have been studied. Due to the different visible-light response range of g-C₃N₄ ($\lambda < 460$ nm) and Ag₂CrO₄ ($\lambda < 680$ nm), the light equipped with a 610 nm optical filter ($\lambda > 610$ nm; ZVL0610, Asahi Spectra Co.) which can only induces band-gap excitation of Ag₂CrO₄ was introduced to evaluate the change of photocatalytic activities and photoelectrochemical properties of the composite. As shown in Fig. 14a, under irradiation with visible light ($\lambda > 420$ nm), both g-C₃N₄ and Ag₂CrO₄ can be

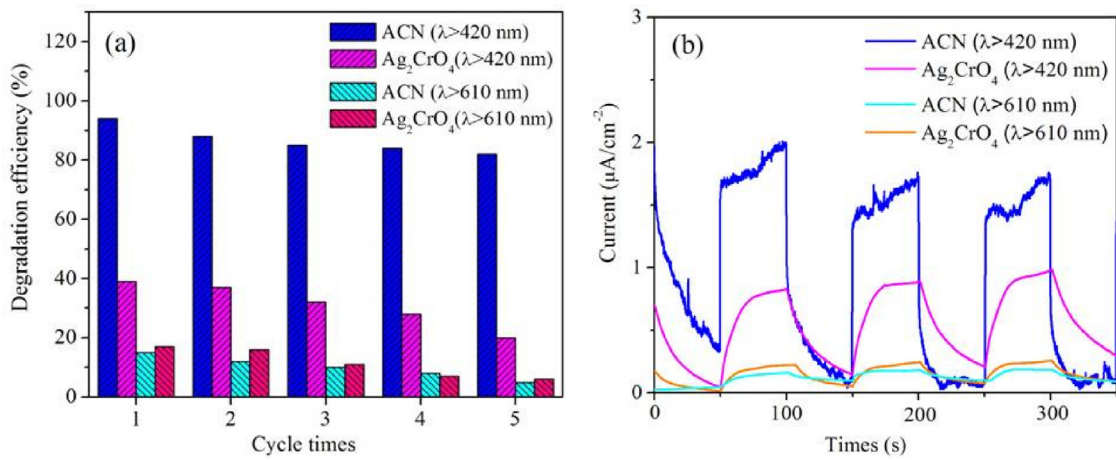


Fig. 14. Comparison of (a) photocatalytic activities and (b) transient photocurrent density of various samples under irradiation with different wavelength light.

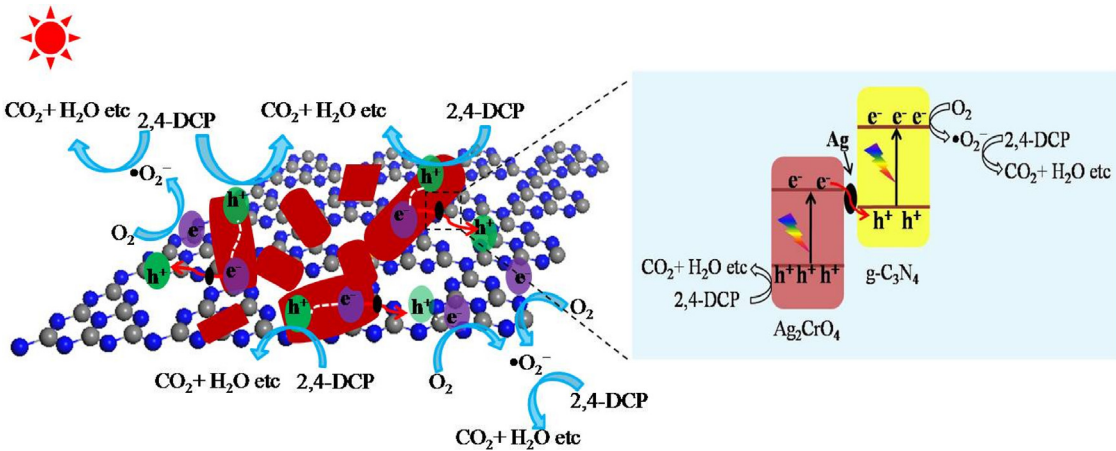


Fig. 15. Mechanism schematic diagram for the photocatalytic 2,4-DCP degradation over $\text{Ag}_2\text{CrO}_4/\text{Ag}/\text{g-C}_3\text{N}_4$ under visible light irradiation.

excited. An obvious deactivation of the photocatalytic activity of pristine Ag_2CrO_4 can be observed after five cycling test, which may caused by the photocorrosion of Ag_2CrO_4 . It has been reported that the Ag^+ in Ag_2CrO_4 can be reduced into metallic Ag by the photogenerated electrons of Ag_2CrO_4 , resulting in decomposition of Ag_2CrO_4 and the loss of the photocatalytic activity [31,45]. In contrast, the composite exhibits stable and enhanced photocatalytic activity in compared with pristine Ag_2CrO_4 , indicating that the photocorrosion of Ag_2CrO_4 is inhibited in the formed heterojunction composite and further verifying that the photoinduced electrons of Ag_2CrO_4 might be transferred into $\text{g-C}_3\text{N}_4$ through the interface formed Ag instead of staying in Ag_2CrO_4 . Moreover, in order to confirm the above speculation, the photocatalytic activities of the composite and Ag_2CrO_4 under visible light ($\lambda > 610$ nm) irradiation were investigated. In this case, only component part Ag_2CrO_4 of the composite can be excited. Results in Fig. 14a and b show that both of the composite and pristine Ag_2CrO_4 display certain photocatalytic activity toward 2,4-DCP degradation. However, the photocatalytic activities of the composite and Ag_2CrO_4 are apparently decreased in compared with the counterparts under visible light ($\lambda > 420$ nm) irradiation and cycling experiment result reveals that the photocatalytic performance of the composite and pristine Ag_2CrO_4 declined after five runs. The photocurrent intensities of the composite and Ag_2CrO_4 are obvious lower than that of the counterparts under visible light ($\lambda > 420$ nm) irradiation respectively. The above results indicate that both of the band-gap excitation of $\text{g-C}_3\text{N}_4$ and Ag_2CrO_4 were indispensable for the high photo-

catalytic activity of $\text{Ag}_2\text{CrO}_4/\text{Ag}/\text{g-C}_3\text{N}_4$ composite toward 2,4-DCP degradation and the photoexcited $\text{g-C}_3\text{N}_4$ can accept the phogenerated electrons produced by Ag_2CrO_4 through the formed Ag at the interface between $\text{g-C}_3\text{N}_4$ and Ag_2CrO_4 . The photoinduced charge transfer routine in the $\text{Ag}_2\text{CrO}_4/\text{Ag}/\text{g-C}_3\text{N}_4$ hybrids follows the Z-scheme mechanism.

As depicted in Fig. 15, the Ag nanoparticles formed in the $\text{Ag}_2\text{CrO}_4/\text{g-C}_3\text{N}_4$ composite might act as electron mediators, the photogenerated electrons in the CB of Ag_2CrO_4 can migrate to the metallic Ag and recombine with the photogenerated holes in the VB of $\text{g-C}_3\text{N}_4$, boosting photogenerated charge separation of the composite. Meanwhile, the strong reducibility of photogenerated electrons in the CB of $\text{g-C}_3\text{N}_4$ and high oxidation ability of photogenerated holes in the VB of Ag_2CrO_4 can be retained to participate in redox reaction. Since the CB level of $\text{g-C}_3\text{N}_4$ is negative than the $\bullet\text{O}_2^-/\text{O}_2$ potential, the adsorbed O_2 on the surface of $\text{g-C}_3\text{N}_4$ can be reduced to $\bullet\text{O}_2^-$ by the photoinduced electrons in the CB of $\text{g-C}_3\text{N}_4$, thus the 2,4-DCP can be decomposed into CO_2 and H_2O by reacting with photogenerated holes in the VB of Ag_2CrO_4 or $\bullet\text{O}_2^-$ produced by photogenerated electrons in the CB of $\text{g-C}_3\text{N}_4$ and the photogenerated charge transfer could be followed Z-scheme mechanism.

4. Conclusions

In conclusion, $\text{Ag}_2\text{CrO}_4/\text{Ag}/\text{g-C}_3\text{N}_4$ heterostrucuture composites have been successfully constructed by using facile in-situ growth strategy and photoreduction process in a two-step method and

exhibit superior photocatalytic activity toward 2,4-DCP degradation under visible light irradiation and the kinetic constant over 10% Ag₂CrO₄/Ag/g-C₃N₄ is 0.91 h⁻¹ which is about 5.2 times as high as that of g-C₃N₄ alone. The reactive species trapping experiments indicate that the •O₂⁻ and photogenerated holes are the main active species. By combining the results of reactive species trapping experiments, ESR analysis and the estimation of band edge position, it reveals that the significant enhancement on photocatalytic performance of the composite is attributed to Z-scheme charge transfer mode, which boosting photoinduced charge separation and enabling the high redox ability of the photocatalyst system. The design principle in this work can be extended to construct other g-C₃N₄-based heterostructure photocatalytic systems for environmental remediation applications.

Notes

The authors declare no competing financial interests.

Acknowledgments

This work was financially supported by National Natural Science Foundation of China (No. 21590813) and the Programme of Introducing Talents of Discipline to Universities (B13012).

References

- [1] X.C. Wang, K. Maeda, A. Thomas, K. Takanabe, G. Xin, K. Domen, M. Antonietti, *Nat Mater.* 8 (2009) 76–80.
- [2] J. Sun, J. Zhang, M. Zhang, M. Antonietti, X. Fu, X.C. Wang, *Nat. Commun.* 3 (2012) 1132–1139.
- [3] X.C. Wang, X.F. Chen, A. Thomas, X.Z. Fu, M. Antonietti, *Adv. Mater.* 21 (2009) 1609–1612.
- [4] W.J. Ong, L.L. Tan, Y.H. Ng, S.T. Yong, S.P. Chai, *Chem. Rev.* 116 (2016) 7159–7329.
- [5] G. Liu, P. Niu, C. Sun, S.C. Smith, Z. Chen, G.Q. Lu, H.M. Cheng, *J. Am. Chem. Soc.* 132 (2010) 1642–11648.
- [6] G.G. Zhang, M.W. Zhang, X.X. Ye, X.Q. Qiu, S. Lin, X.C. Wang, *Adv. Mater.* 26 (2014) 805–809.
- [7] Y. Zheng, L.H. Lin, X.J. Ye, F.S. Guo, X.C. Wang, *Angew Chem. Int. Ed.* 53 (2014) (1930) 11926–11930.
- [8] H.X. Zhao, H.T. Yu, X. Quan, S. Chen, H.M. Zhao, H. Wang, *RSC Adv.* 4 (2014) 624–628.
- [9] J. Liu, Y. Liu, N.Y. Liu, Y.Z. Han, X. Zhang, H. Huang, Y. Lifshitz, S.T. Lee, J. Zhong, Z.H. Kang, *Science.* 347 (2015) 970–974.
- [10] H. Wang, Y. Su, H.X. Zhao, H.T. Yu, S. Chen, Y.B. Zhang, X. Quan, *Environ. Sci. Technol.* 48 (2014) 11984–11990.
- [11] V.W. Lau, M.B. Mesch, V. Doppel, V. Blum, J. Senker, B.V. Lotsch, *J. Am. Chem. Soc.* 137 (2015) 1064–1072.
- [12] W.J. Wang, J.C. Yu, D.H. Xia, P.K. Wong, Y.C. Li, *Environ. Sci. Technol.* 47 (2013) 8724–8732.
- [13] Y.P. Yuan, S.W. Cao, Y.S. Liao, L.S. Yin, C. Xue, *Appl. Catal. B: Environ.* 140–141 (2013) 164–168.
- [14] Roland Marschall, *Adv. Funct. Mater.* 24 (2014) 2421–2440.
- [15] H.J. Li, Y. Zhou, W.G. Tu, J.H. Ye, Z.G. Zou, *Adv. Funct. Mater.* 25 (2015) 998–1013.
- [16] W. Liu, M.L. Wang, C.X. Xu, S.F. Chen, X.L. Fu, *J. Mol. Catal. A: Chem.* 368 (2013) 9–15.
- [17] J.X. Sun, Y.P. Yuan, L.G. Qiu, X. Jiang, A.J. Xie, Y.H. Shen, J.F. Zhu, *Dalton Trans.* 41 (2012) 6756–6763.
- [18] L.Q. Ye, J.Y. Liu, Z. Jiang, T.Y. Peng, L. Zan, *Appl. Catal. B: Environ.* 142–143 (2013) 1–7.
- [19] C.S. Pan, J. Xu, Y.J. Wang, D. Li, Y.F. Zhu, *Adv. Funct. Mater.* 22 (2012) 1518–1524.
- [20] P. Zhou, J.G. Yu, M. Jaroniec, *Adv. Mater.* 26 (2014) 4920–4935.
- [21] Y.X. Yang, Y. Guo, W. G., Y.H. Zhao, X. Yuan, Y.H. Guo, *J. Hazard Mater.* 271 (2014) 150–159.
- [22] W.B. Li, C. Feng, S.Y. Dai, J.G. Yue, F.X. Hua, H. Hou, *Appl. Catal. B: Environ.* 168–169 (2015) 465–471.
- [23] D. Ma, J. Wu, M.C. Gao, Y.J. Xin, T.J. Ma, Y.Y. Sun, *Chem. Eng. J.* 290 (2016) 136–146.
- [24] Y.M. He, L.H. Zhang, B.T. Teng, M.H. Fan, *Environ. Sci. Technol.* 49 (2015) 649–656.
- [25] X.F. Yang, Z.P. Chen, J.S. Xu, H. Tang, K.M. Chen, Y. Jiang, *Appl. Mater. Interfaces.* 7 (2015) 15285–15293.
- [26] S.X. Ouyang, Z.S. Li, Z. Ouyang, T. Yu, J.H. Ye, Z.G. Zou, *J. Phys. Chem. C.* 112 (2008) 3134–3141.
- [27] Y. Liu, H.B. Yu, M. Cai, J.W. Sun, *Catalysis Commun.* 26 (2012) 63–67.
- [28] F. Soofivand, F. Mohandes, M.S. Niasari, *Materials Research Bulletin.* 48 (2013) 2084–2094.
- [29] D.F. Xu, B. Cheng, J.F. Zhang, W.K. Wang, J.G. Yu, W.K. Ho, *J. Mater. Chem. A.* 3 (2015) 20153–20166.
- [30] J.F. Zhang, W.L. Yu, J.J. Liu, B.S. Liu, *Applied Surf. Sci.* 358 (2015) 457–462.
- [31] D.F. Xu, B. Cheng, S.W. Cao, J.G. Yu, *Appl. Catal. B: Environ.* 164 (2015) 380–388.
- [32] G.Z. Liao, S. Chen, X. Quan, H.T. Yu, H.M. Zhao, *J. Mater. Chem.* 22 (2012) 2721–2726.
- [33] J.C. Wang, H.C. Yao, Z.Y. Fan, L. Zhang, J.S. Wang, S.Q. Zang, Z.J. Li, *ACS Appl. Mater. Interfaces.* 8 (2016) 3765–3775.
- [34] R.Q. Ye, H.B. Fang, Y.Z. Zheng, N. Li, Y. Wang, X. Tao, *ACS Appl. Mater. Interfaces.* 8 (2016) 13879–13889.
- [35] Z.Y. Zhang, J.D. Huang, M.Y. Zhang, Q. Yuan, B. Dong, *Appl. Catal. B: Environ.* 163 (2015) 298–305.
- [36] J.G. Hou, Z. Wang, C. Yang, W.L. Zhou, S.Q. Jiao, H.M. Zhu, *J. Phys. Chem. C.* 117 (2013) 5132–5141.
- [37] X.J. Bai, R.L. Zong, C.X. Li, D. Liu, Y.F. Liu, Y.F. Zhu, *Appl. Catal. B: Environ.* 147 (2014) 82–91.
- [38] M.L. Pang, J.Y. Hu, H.C. Zeng, *J. Am. Chem. Soc.* 132 (2010) 10771–10785.
- [39] K. Lundholm, D. Bostrom, A. Nordin, A. Shchukarev, *Environ. Sci. Technol.* 41 (2007) 6534–6540.
- [40] Z.Z. Lin, X.C. Wang, *Angew. Chem. Int. Ed.* 52 (2013) 1735–1738.
- [41] J.L. Wang, Y. Yu, L.Z. Zhang, *Appl. Catal. B: Environ.* 136–137 (2013) 112–121.
- [42] J. Shang, W.C. Hao, X.J. Lv, T.M. Wang, X.L. Wang, Y. Du, S.X. Dou, T.F. Xie, D.J. Wang, J.O. Wang, *ACS Catal.* 4 (2014) 954–961.
- [43] S.F. Chen, Y.F. Hu, S. G. Meng, X.L. Fu, *Appl. Catal. B: Environ.* 150–151 (2014) 564–573.
- [44] Y.Z. Hong, Y.H. Jiang, C.S. Li, W.Q. Fan, X. Yan, M. Yan, W.D. Shi, *Appl. Catal. B: Environ.* 180 (2016) 663–673.
- [45] G.P. Dai, J.G. Yu, G. Liu, *J. Phys. Chem. C* 116 (2012) 15519–15524.